



Synthesis of $\text{g-C}_3\text{N}_4$ by different precursors under burning explosion effect and its photocatalytic degradation for tylosin



Hao Dong^{a,b}, Xuetao Guo^{a,d,*}, Chen Yang^c, Zhuozhi Ouyang^c

^a College of Natural Resources and Environment, Northwest A&F University, Yangling, Shaanxi, 712100, China

^b School of Earth and Environment, Anhui University of Science and Technology, Huainan, 232001, China

^c College of Environment and Energy, South China University of Technology, Guangzhou, 510006, China

^d Key Laboratory of Plant Nutrition and the Agri-Environment in Northwest China, Ministry of Agriculture, Yangling, Shaanxi, 712100, China

ARTICLE INFO

Keywords:

Sodium nitrate

$\text{g-C}_3\text{N}_4$

Surface modification

Tylosin

Photocatalytic

ABSTRACT

The use of abundant sunlight for semiconductor photo-degradation of antibiotics is an ideal way to solve global water pollution. Here, the sodium nitrate modified photocatalysts exhibits enhanced photocatalytic efficiency for degradation of tylosin under simulated sunlight irradiation over $\text{g-C}_3\text{N}_4$ alone. In addition, the pure $\text{g-C}_3\text{N}_4$ and sodium nitrate modified $\text{g-C}_3\text{N}_4$ photocatalysts were investigated in terms of their crystal structures, morphologies, optical properties by using XRD, SEM, TEM, Raman, FTIR, UV-vis and XPS. On the basis of these results, the morphology dependence of the visible light absorption and the photocatalytic efficiency under simulated sunlight irradiation has been systematically investigated. It was found that the type of precursors and the molar ratio of sodium nitrate have an evident impact on the crystal structure of $\text{g-C}_3\text{N}_4$, and photocatalytic performance due to varied reaction pathways and degree of condensation. The photocatalytic activity evaluated under simulated sunlight indicates that the as-synthesized photocatalysts is effective in obtaining the energy of solar spectrum and transforming it into the chemical energy for tylosin degradation.

1. Introduction

Water is the fountain of life. Especially for humans, clean and safe water is the basic standards of our modern life. However, many organic contaminants are frequently detected in water, for example like antibiotics are one of the most commonly detected contaminants from surface water [1–3]. At present, antibiotics residues are frequently detected in a wide range of environmental samples, especially in treated wastewater and even drinking water [4–6]. The residual antibiotics are thrown to water courses and soils, even in low concentration, may lead to the emergence of drug resistance among pathogenic microbes, and even result in the formation of cross- and multiple- resistances in organisms [7,8]. Therefore, the occurrence and transfer of antibiotics in the environment is recognized as one of the most serious global threats to human and animal health [3,5]. However, the presence of different antibiotics in the wastewater treatment plant has been found in concentrations of the order of $\mu\text{g L}^{-1}$ and ng L^{-1} , showing that the conventional wastewater treatments are not effective for their removal [9–11]. Therefore, it is importance to develop an environmentally friendly strategy for the removal of antibiotics in contaminated waters.

Until now, different techniques are applied to remove antibiotics

from waste water, such as sorption, photocatalytic degradation, oxidation and biodegradation. Among them, photocatalytic degradation is considered as one of the most promising methods because of its high efficiency, eco-friendly character and low cost [12–16]. Recently, graphitic carbon nitride ($\text{g-C}_3\text{N}_4$), as an environmentally-friendly organic semiconductor, has attracted worldwide attentions [17]. This material can be prepared easily through thermal polymerization of different nitrogen-rich precursors such as melamine, urea, dicyandiamide and thiourea [18,19]. $\text{g-C}_3\text{N}_4$ possesses a high chemical and thermal stability as well as unique optical and electronic properties [20]. Up to now, $\text{g-C}_3\text{N}_4$ has been used as a photocatalyst to reduce CO_2 , generate hydrogen from water and decompose pollutants [21–24]. However, the photocatalytic efficiency of bulk $\text{g-C}_3\text{N}_4$ is limited because of its fast charge recombination, low surface-to-volume ratio, and weak redox ability [25,26]. To improve the photocatalytic activity of $\text{g-C}_3\text{N}_4$, many strategies have been proposed by increasing of the surface-to-volume ratio, changing morphology, combining with other semiconductors and doping metal/non-metal ions [15,19,27–30]. Among these methods, changing morphology and crystal structure of $\text{g-C}_3\text{N}_4$ can increase the number of active sites, which is beneficial for the photocatalytic degradation [31,32]. In addition, a large number of

* Corresponding author at: College of Natural Resources and Environment, Northwest A&F University, Yangling, Shaanxi, 712100, China.

E-mail address: guoxuetao2005@nwsuaf.edu.cn (X. Guo).

studies showed that the morphology of $\text{g-C}_3\text{N}_4$ nanostructures is crucial for photocatalysis performance [31]. The study of Yang et al. also showed that the photocatalytic activity of acidified $\text{g-C}_3\text{N}_4/\text{g-C}_3\text{N}_4$ hybrids with enhanced photocatalytic activity, which is due to change morphology and construction of heterostructure with a higher specific surface area [33]. In addition, Chen et al. reported the modification of $\text{g-C}_3\text{N}_4$ with hydrazine hybrid, and they found that the diazanyl group was successfully introduced onto the $\text{g-C}_3\text{N}_4$ surface, which influences the surface structure, optical properties, electronic structure and energy band of $\text{g-C}_3\text{N}_4$ [34]. Therefore, preparing structure distortion $\text{g-C}_3\text{N}_4$ with a special crystal structure is important significance for improving the photocatalysis performance.

Sodium nitrate at high temperatures have a strong oxidative and burning explosion properties, and will decompose to generate a large amount of gas [35]. In addition, sodium nitrate may disrupt some of the chemical bonds in the synthesis of $\text{g-C}_3\text{N}_4$ and alter its structure and morphology by burning explosion. In this study, photocatalyst was prepared by a modified thermal polymerization approach using sodium nitrate as an oxidizing agent. Herein, an attempt was made to synthesize $\text{g-C}_3\text{N}_4$ by thermal decomposition of melamine, dicyandiamide and urea [36]. Tylosin (TYL), one of the most widely used antibiotics in therapeutics and growth promoters in the whole world, was selected as a model compound to investigate the photocatalytic degradation behavior of antibiotics in aqueous solution [37,38]. The experiment focuses on the molar ratio of sodium nitrate and different precursor, as well as the impact of time on photo-degradation rate. In addition, the effect of sodium nitrate modification on the structure and photocatalytic activity of $\text{g-C}_3\text{N}_4$ was systematically studied. Based on these results, a mechanism for the enhanced photocatalytic performance over as-synthesized photocatalyst was proposed.

2. Materials and methods

2.1. Reagents

TYL tartrate (MW 916.14 g/mol, purity > 95%) was used as bought from Sigma-Aldrich Corporation [39]. Melamine, dicyandiamide, urea and sodium nitrate were obtained from Sinopharm Chemical Reagent Company. All other materials used in this study were analytical grade and used without further treatment.

2.2. Samples preparation

The $\text{g-C}_3\text{N}_4$ samples were synthesized by a thermal polymerization method using urea, dicyandiamide and melamine as reagents [36]. The modified $\text{g-C}_3\text{N}_4$ with desired nanoscale and different morphology can be directly synthesized by thermal polymerization. Typically, CNM-3 was synthesized as follows: sodium nitrate (1.123 g) and melamine (5 g) were mixed and transferred into a semiclosed crucible with a cover. The crucible was heated up to 500 °C for 2 h and then extended to 550 °C for 2 h with a heating rate of 10 °C min⁻¹ in a muffle furnace. The obtained product was denoted as CNM-x, where x stands for the molar ratio of melamine to sodium nitrate. Samples with other different molar ratios of melamine (5, 10, 20, 30) to sodium nitrate have been synthesized by the same method mentioned above and noted as CNM-5, CNM-10, CNM-20 and CNM-30, respectively. Other precursors (urea, dicyandiamide) were also used to synthesize modified $\text{g-C}_3\text{N}_4$ sample by the similar method, and the as-synthesized samples were denoted as CNU-x and CND-x, respectively.

2.3. Photocatalytic activity measurements

The photocatalytic activity of the synthesized samples for the degradation of TYL was evaluated under simulated sunlight irradiation. The photo-degradation experiments were performed in a self-made reactor under irradiation of 300 W Xe lamp. In the degradation reactions,

0.1 g photocatalyst was dispersed in 200 mL TYL (5 mg/L) solution with vigorous stirring and ensure uniform irradiation of the catalyst suspension during the experiment process. Before the light irradiation, the mixed solution was stirred in the dark for 12 h to reach the adsorption/desorption equilibrium. At a certain point of time, about 1 mL solutions were collected from the suspension and the photocatalyst was removed from the solution by filtration with a 0.45 μm filter membranes. Finally, 1 mL of solutions was transferred to an amber glass bottle for detection.

The photocatalytic degradation process can be well fitted by pseudo first-order kinetics (Eq. (1)), thus the first-order rate constant (k) is used to compare the photodegradation efficiency of all photolysis experiments [40,41]:

$$\ln(C_0/C) = kt \quad (1)$$

2.4. Chemical analysis

A reverse-phase high-performance liquid chromatography (Hitachi D-2000 Elite-HPLC) with a C₁₈ column (5 μm, 4.6 × 250 mm; Agilent) and a diode array UV detector (wavelength at 290 nm for tylosin) to quantify TYL from aqueous solution. The mobile phase (at a flow rate of 1 mL min⁻¹) for tylosin was a mixture of acetonitrile (35%) and an aqueous solution (65%) adjusted to pH = 2.0 with 0.01 mol L⁻¹ KH₂PO₄.

3. Results and discussion

3.1. Evolution of structure and morphology

The XRD patterns of CNM-x, CND-x and CNU-x samples synthesized at different precursors are shown in Fig. 1. Two typical diffraction peaks are discovered in the XRD patterns for all samples, indicating the successful synthesis of $\text{g-C}_3\text{N}_4$ by thermal polymerization of three different precursors [19,33,42]. A minor angle diffraction peak at 13.2° corresponded to tri-s-thiazine units (100), and the strong peak at 27.5° accorded with the repeated the inter-layer stacking of conjugated aromatic systems, which is indexed for graphitic materials as the (002) peak [43,44]. Notably, With the sodium nitrate effect, the intensity of the sharp (100) diffraction gradually decreased and the peak shape broadened (Fig. 1a–c). The XRD patterns of CND-x and CNM-x still contained the characteristic (100) interlayer-stacking peak, suggesting the graphite-like structure of $\text{g-C}_3\text{N}_4$ was still retained after the thermal decomposition treatment with sodium nitrate. However, for CNU-x, the intensities of peaks corresponding to (100) has disappeared. This reflects that the presence of sodium nitrate prevent the polymerization of precursors (melamine, dicyandiamide, urea) and the stacking (crystallization) of $\text{g-C}_3\text{N}_4$ sheets. In addition, an obvious right-shift toward a higher 2θ value is observed for all the sodium nitrate modification $\text{g-C}_3\text{N}_4$ catalysts (inset of Fig. 1a–c). Further observations found that the characteristic peaks (002) appeared in 27.82°, 27.70° and 27.88° for CND-5, CNM-3 and CNU-30, respectively. This is due to the strong interaction between $\text{g-C}_3\text{N}_4$ and sodium nitrate, which leads to the formation of defects and the reduction of lattice distances [45]. In addition, crystal lattice distortion may be attributed to Na can inhibit crystal growth [46]. Whereas, the diffraction peaks of all the CNU-x samples are weaker and more extensive than CNM, indicating the presence of smaller crystalline domains (Fig. 1d) [47]. The results show that compared with the other two precursors, O-containing precursor (urea) can be more compact $\text{g-C}_3\text{N}_4$ structure [48].

The morphologies and microstructures of CND-5, CNM-3 and CNU-30 were investigated by SEM and TEM. Fig. 2(a and b) show the flat and layered structure of the synthesized CND and CNM, Which is consistent with the observation of others in the literature [41]. In addition, CNU composes a number of irregular flake particles with the layered structure [49]. Compared with the flaky layered structure of the pristine g-

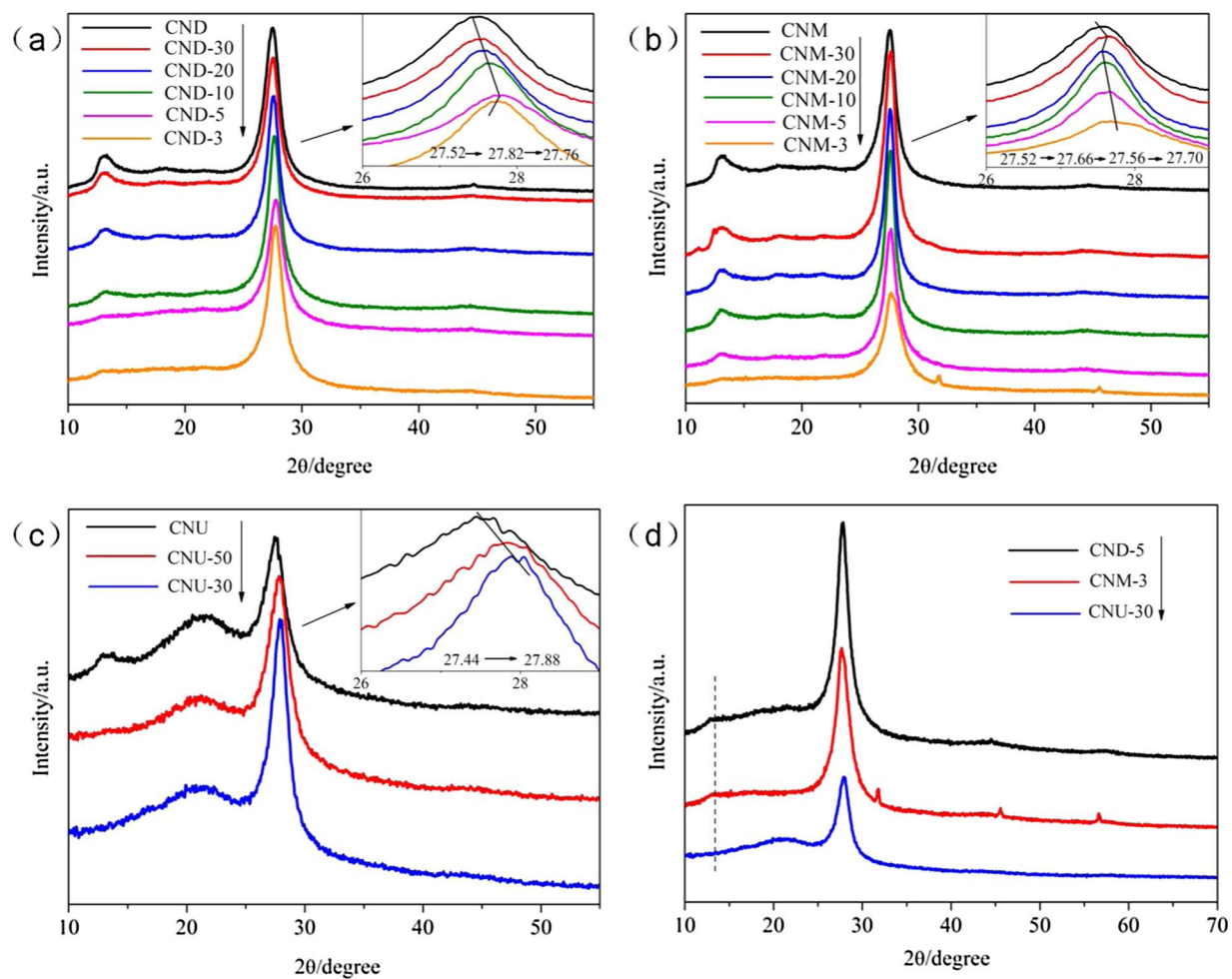


Fig. 1. XRD patterns of CND-x(a), CNM-x(b), and CNU-x(c) (enlarged profile of the dominant (002) peak), (d)XRD high-resolutions of CND-5,CNM-3 and CNU-30.

C_3N_4 , all the $\text{g-C}_3\text{N}_4$ after the burning explosion effect showed an irregular massive structure. As illustrated in Fig. 2(g–i), it was evident that lots of fragments covered on the surface of all samples, and the CNU-30 surface is the most prominent. Compared to CND-5 with a compact microstructure (Fig. 2j and l), the as-prepared CNU-30 sample consists of the ultrathin two-dimension layers with abundant of pores, caused by the gas released by sodium nitrate and urea during high temperature calcination process. The difference in morphology and microstructure between CND-5 and CNM-3 are also observed from their SEM images. CNM-3 compared to the other two kinds of catalysts, the CNM-3 samples show larger diameter pores and dimensions, which may be attributed to the structure of melamine to release less gas during thermal polymerization. The above observation results show that the surface of CNU-30 is deformed and curled due to the addition of sodium nitrate, and the thin layer structure is gradually formed. This result can be further confirmed by its TEM image. Typical TEM image of modified carbon nitride shows multi-layer structure containing abundant non-uniform pore networks (Fig. 3), which is attributed to the synergistic effect of sodium nitrate on the thermal polymerization process with the precursors [50]. Notably, CNU-30 presents smaller particles and thinner sheets relative to CNM-3. The TEM image of CNU-30 shown in Fig. 3f exhibits that the CNU-30 has a porous structure due to a large amount of gas emissions during thermal polymerization.

To further observe the surface area and porous structure of $\text{g-C}_3\text{N}_4$ modification, the as-synthesized samples were analyzed by BET (Fig. 4). It can be seen that all samples have similar nitrogen adsorption-desorption isotherms, and all belong to the Type IV isotherm [51]. According to the nitrogen adsorption/desorption isotherms, the BET

surface areas were found 7.012, 3.219, 4.129, 2.547, 53.818 and $4.556 \text{ m}^2/\text{g}$ for CND, CND-5, CNM, CNM-3, CNU and CNU-30, respectively. Clearly, after thermal polymerization treatment with the participation of sodium nitrate, all the $\text{g-C}_3\text{N}_4$ has a significant reduction in specific surface area. In addition, the pore volume decrease with the participation of sodium nitrate, meaning that the $\text{g-C}_3\text{N}_4$ layer spacing will be reduced at the presence of sodium nitrate. The modified $\text{g-C}_3\text{N}_4$ samples has a relative smaller surface area and pore volume may be attributed to the sintering effect of sodium nitrate in the process of thermal polymerization, which is consistent with the XRD and TEM observations [52,53]. Furthermore, by SEM images and BET analysis, it can be found that sodium nitrate can inhibit the formation of large specific surface area, but can change the morphology and crystal structure of $\text{g-C}_3\text{N}_4$ to promote the separation of electron-hole pairs.

The FTIR spectra indicate the functional groups present in the CNM-x (Fig. 5-a), CND-x (Fig. 5-b) and CNU-x (Fig. 5-c). As seen in Fig. 5, all samples basically maintain the classic $\text{g-C}_3\text{N}_4$ structure. They showed several major bands centered at about 3000–3500, 2178, 1200–1700 and 806 cm^{-1} . In comparison with $\text{g-C}_3\text{N}_4$, all as-prepared catalysts samples showed similar absorptions in the wavenumber range of 1200–1700 cm^{-1} that were the stretching vibrations of conjugated CN rings and the characteristic breathing mode of s-triazine at 806 cm^{-1} [15,54–56]. The 2178 cm^{-1} peak can be assigned to $\text{C}\equiv\text{N}$ triple bonds, its intensity increased with addition of sodium nitrate, indicating that the aromatic unit of $\text{g-C}_3\text{N}_4$ was partly broken by burning explosion effect [44,57–59]. Whereas, an apparent difference was found in the 3000–3500 cm^{-1} range, where the absorption band at 3170 cm^{-1} was ascribed to the stretching mode of O–H and the band at 3430 cm^{-1} can

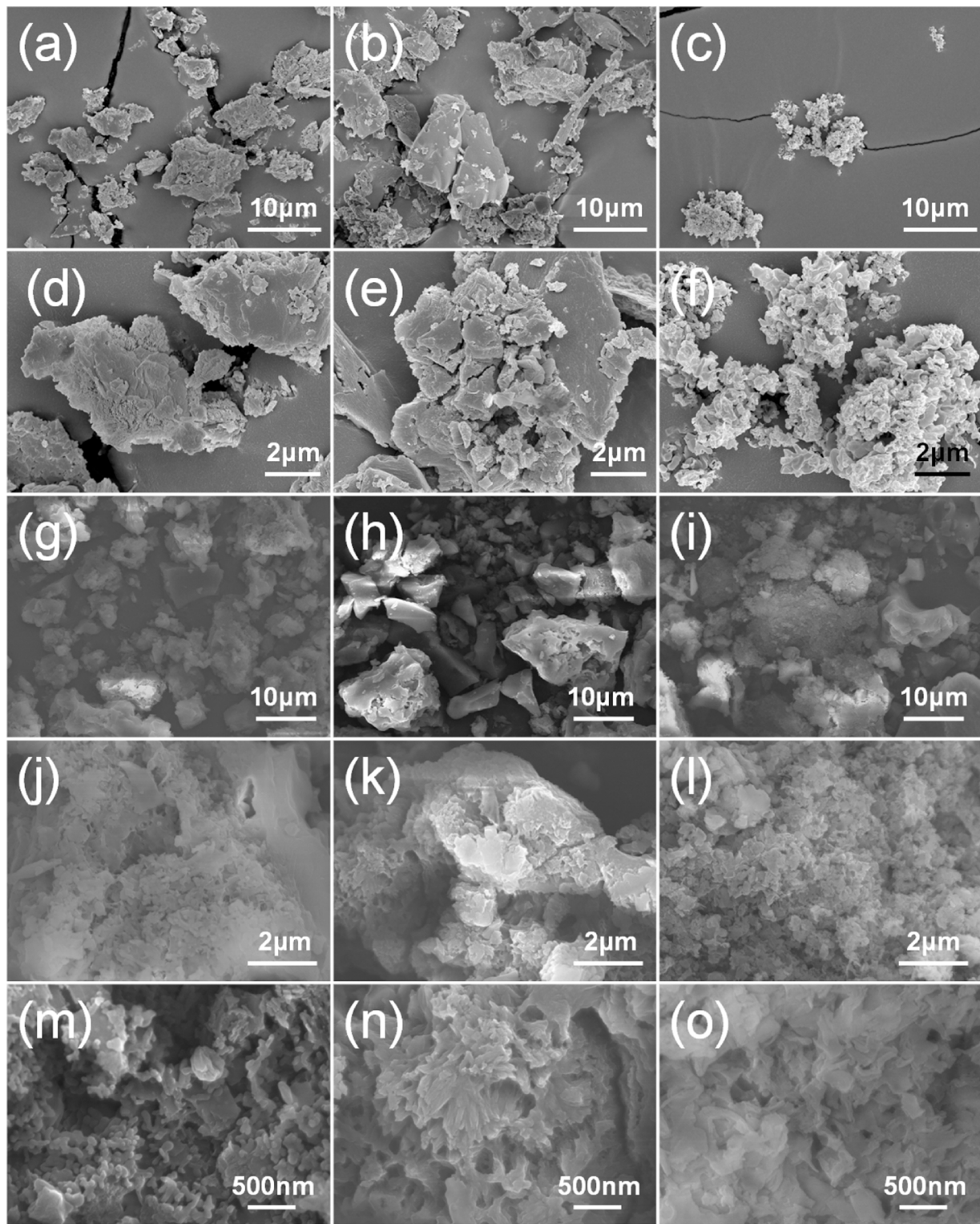


Fig. 2. SEM images of CND(a, d), CNM(b, e), CNU(c, f), CND-5 (g, j, m), CNM-3 (h, k, n) and CNU-30 (i, l, o).

be attributed to the N–H vibration mode [55]. For CND-x and CNM-x, it is seen that the peak at 3170 cm^{-1} of modified $\text{g-C}_3\text{N}_4$ is weaker than that of unmodified $\text{g-C}_3\text{N}_4$, showing that the hydroxyl groups on the $\text{g-C}_3\text{N}_4$ surface are eliminated by modification of sodium nitrate. In addition, modified catalyst has weak peaks between 3100 and 3450 cm^{-1} comparing to unmodified catalyst which correspond to the remnant $-\text{NH}_2$ and $-\text{NH}-$ groups [60]. The emergence of new functional groups can be attributed to the burning explosion effect of the precursors

during thermal polymerization.

To investigate the surface composition and chemical state of different element, CND-5, CNM-3 and CNU-30 were analyzed by XPS. The survey scan XPS spectrum (Fig. 6a) displays that the as-synthesized samples contain carbon, nitrogen, oxygen and sodium signals, in which the strength of the N 1s intensity is strongest due to its highest proportion in $\text{g-C}_3\text{N}_4$ samples. In Fig. 6b-d, The XPS spectra show that there is no significant shift in the binding energy of C 1s, N 1s and O 1s,

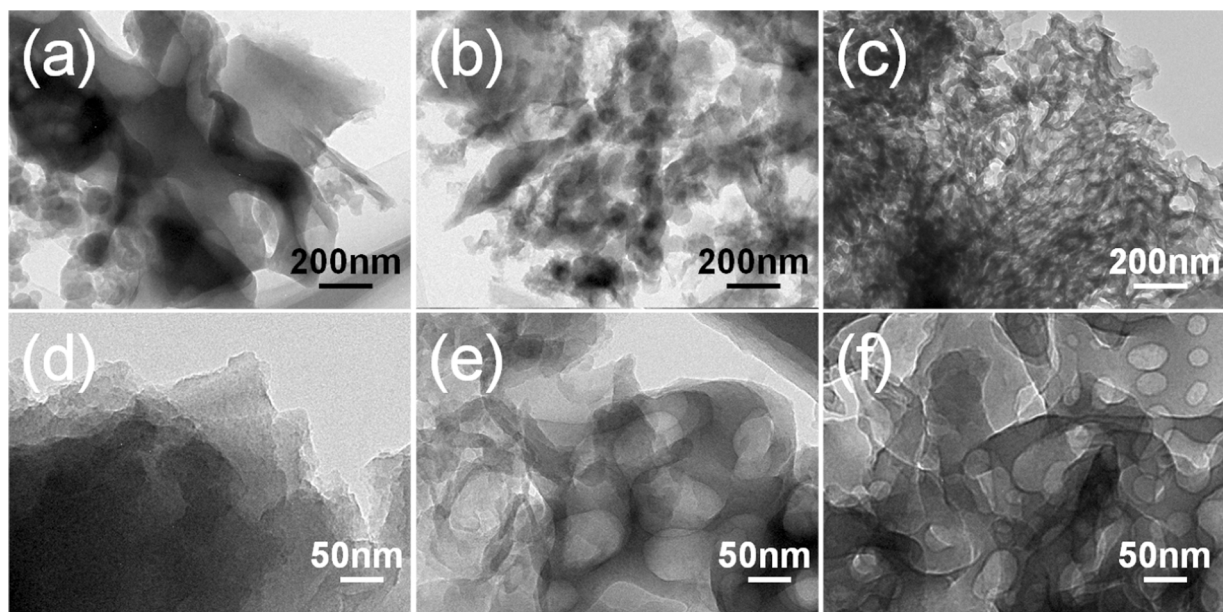


Fig. 3. TEM images of CND-5 (a, d), CNM-3 (b, e), CNU-30 (c, f).

indicating that the chemical state and structure of the $\text{g-C}_3\text{N}_4$ synthesized by the three different precursors are almost the same. The XPS spectra of the C 1s core level for all samples can be deconvoluted into three components including the sp^2 hybridized C atoms C–C (284.59 eV) [44,61], C–O (286.11 eV) and the sp^2 -bonded C in $\text{N}=\text{C}(\text{N})_2$ (288.34 eV) [33,43,50,62]. And the high definition N 1s spectra of all samples can be deconvoluted into two parts of the Fig. 6c, which are characteristic of C=N–C (398.72 eV) and N–(C)₃(400.43 eV) [28,56,63]. The peaks at the position of 404.95 eV may be attributed to the π -excitations [50,58,64]. In addition, the spectrum of O 1s in Fig. 6d can be deconvoluted into two single peaks with binding energies of 531.68 and 533.08 eV that attributed to carbonyl (C=O) group and adsorbed water [56], respectively. As shown in Fig. 6e, the Na 1s spectrum of as-synthesized samples displays only one Na 1s core level at ca. 1071.62 eV, which means that the chemical constituents of the species containing Na are contained in the sample [65].

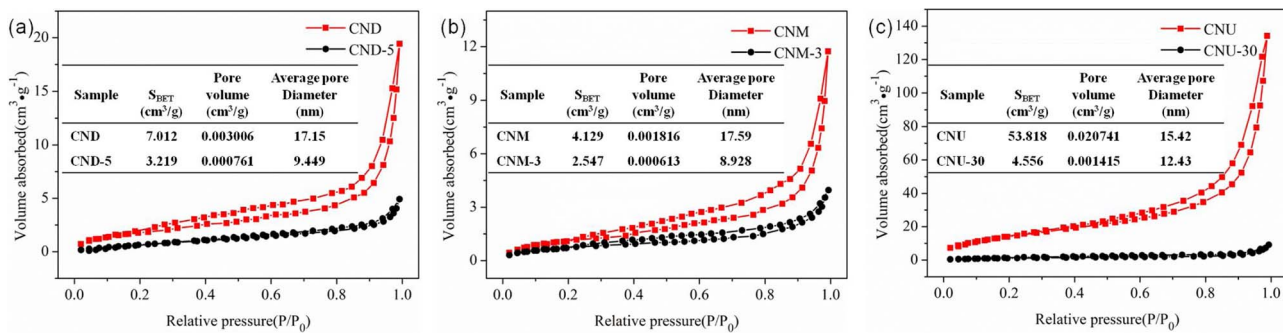
The as-prepared samples are further characterized by Raman spectroscopy. As shown in Fig. 6f, it was clear to observe that CND-5, CNM-3 and CNU-30 polymers exhibited similar Raman vibration modes. The Raman shifts at 400–1300 cm^{-1} were related to the typical heptazine units. The peaks located at 471 cm^{-1} , 720 cm^{-1} , 754 cm^{-1} , 980 cm^{-1} , 1157 cm^{-1} and 1235 cm^{-1} originate from the vibration modes of CN heterocycles in $\text{g-C}_3\text{N}_4$ [66]. In detail, the strong diffraction peaks at 720 and 1235 cm^{-1} are caused by the different types of ring breathing modes of s-triazine [42,67]. The two wide peaks at $\sim 1500 \text{ cm}^{-1}$ are assigned to the D and G bands of a typical graphitic

structure [42]. In addition, the Raman spectrum of all as-prepared samples displayed a peak at 2184 cm^{-1} , which is assigned to N atmospheric stretching vibration [68]. This means that no other significant changes have occurred in the structure of $\text{g-C}_3\text{N}_4$.

3.2. Optical absorption performance and photocatalytic activity

3.2.1. Optical absorption performance

Fig. 7 shows the UV-vis of the CND-x, CNM-x and CNU-x composites. It can be seen from the figure that all the synthesized samples show similar semiconductor adsorption. As for the CND-x, CNM-x and CNU-x nanocomposites, the absorption edge of obtained samples red-shift and improved visible light activation capability can be attributed to the sodium nitrate destroy the surface of $\text{g-C}_3\text{N}_4$ at high temperature. All samples have excellent visible light absorption, the absorption edge of more than 450 nm, which may be due to the synthesis of $\text{g-C}_3\text{N}_4$ samples with different structures and morphology. The red-shift of the absorption wavelength indicated that the modified $\text{g-C}_3\text{N}_4$ could absorb more photons. According to the spectrum, compared with unmodified $\text{g-C}_3\text{N}_4$, the increased absorption intensity of modified $\text{g-C}_3\text{N}_4$ composites in the visible light region is attributed to sodium nitrate modification. Thereafter, the band gap values of the synthesized photocatalysts were calculated by plots of $(\text{ahv})^{1/2}$ versus photo energy. From Fig. 7b, the calculated band gaps of CND, CND-30, CND-20, CND-10, CND-5 and CND-3 were 2.5, 2.38, 2.34, 2.40, 2.53 and 2.55 eV, respectively. In addition, according to the linear-fit lines (Fig. 7d), the band gaps were found 2.50, 2.47, 2.34, 2.33, 2.36 and 2.51 eV for CNM,

Fig. 4. N_2 adsorption-desorption isotherms of CND-x (a), CNM-x(b), and CNU-x(c).

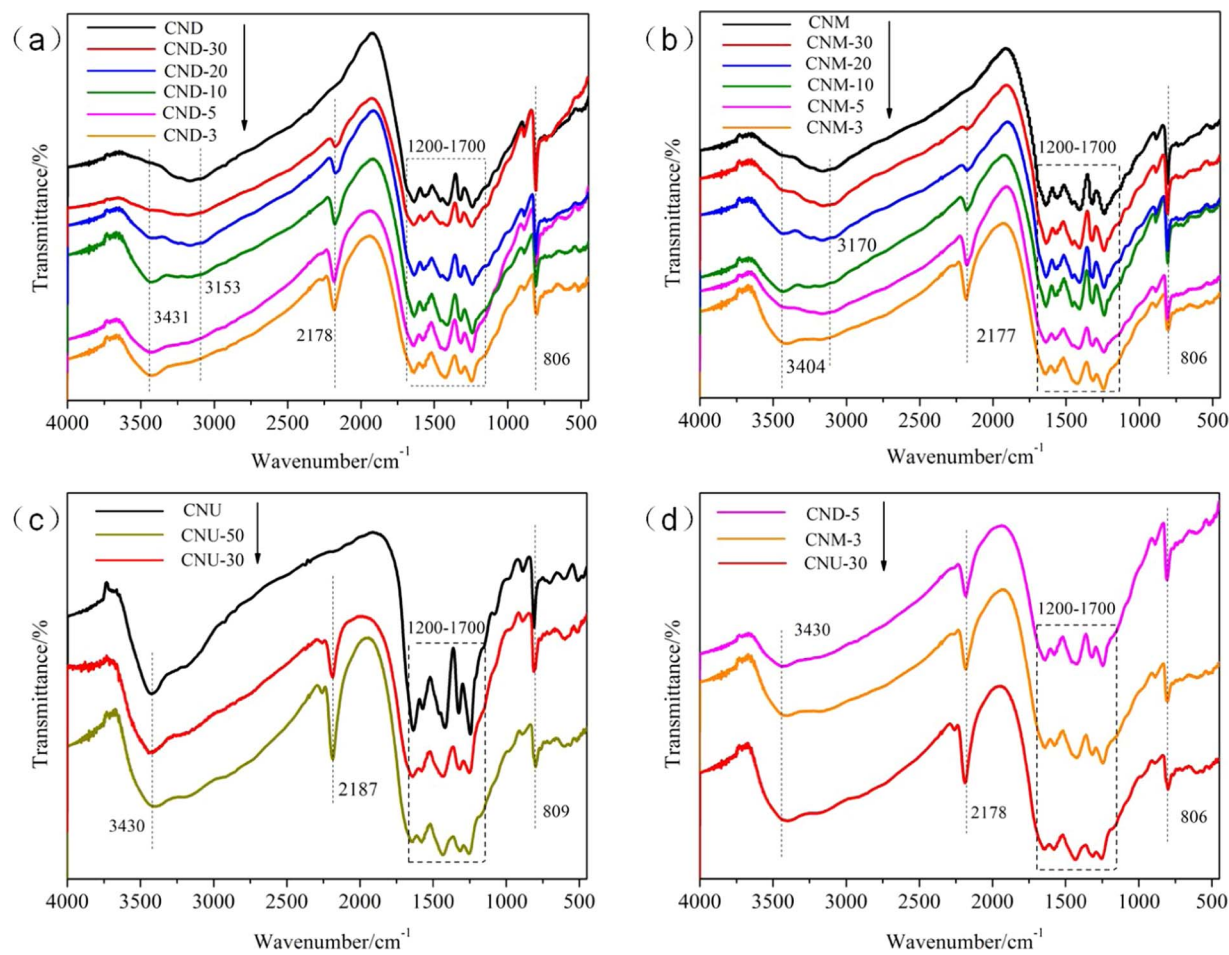


Fig. 5. FTIR high-resolutions of carbon nitride derived from different precursors.

CNM-30, CNM-20, CNM-10, CNM-5 and CNM-3, respectively. At the same time, the band gaps of the CNU decreases as the molar ratio of sodium nitrate increases, and its band gaps decreases from 2.67 to 2.58. The reduction of band gap will capture more visible light and may be beneficial to the enhancement of photodegradation efficiency [42]. Nevertheless, the optical characteristics of photocatalyst does not fully reflect its photocatalytic activity, because the photocatalysis process includes interface photocatalysis, light capture, and photoelectron transition, etc. [69]. Therefore, the further analysis of the photocatalytic performance of the as-synthesized samples is necessary.

3.2.2. Photocatalytic degradation of TYL

The photocatalytic performances of the photocatalysts were evaluated by photocatalytic degrading TYL in aqueous solution under simulated sunlight irradiation. TYL was rarely degraded without photocatalysts, confirming it is resistant to photolysis in water under simulated sunlight irradiation. As shown in Fig. 8, by comparing with pristine $\text{g-C}_3\text{N}_4$, all of the CND-x, CNM-x and CNU-x composites exhibited significantly enhanced higher photocatalytic activity under visible light irradiation. Among these samples, CND-5, CNM-3 and CNU-30 displayed the most prominent activity that photo-decomposed 99% TYL after the 30 min visible light illumination. The kinetic curves of TYL degradation can be approximated as a pseudo-first-order process by Eq. (1). k also increased with the increase of the molar ratio of sodium nitrate modification, indicating that the use of sodium nitrate modified $\text{g-C}_3\text{N}_4$ can enhance photocatalytic activity. The rate constant of CND-5, CNM-3 and CNU-30 is 5.05, 5.32, 12.93 times for unmodified $\text{g-C}_3\text{N}_4$, respectively, firmly proving the active role of the sodium nitrate. This finding means that the sodium nitrate play an significant role

in modified $\text{g-C}_3\text{N}_4$.

In addition, the stability and reusability of catalysts were of significant importance for practical application. Therefore, we tested four successive cycles for the photocatalytic degradation of TYL by CND-5, CNM-3 and CNU-30. Fig. 9 shows that the as-prepared composite material has good recyclability, and there is no significant deactivation of the catalyst after 4 cycles in TYL degradation. The cycling experiments determined the stability and reusability of the samples.

3.2.3. Possible mechanism of photocatalytic activity enhancement

Fig. 10 shows the possible process synthesis of pure $\text{g-C}_3\text{N}_4$ and sodium nitrate modified $\text{g-C}_3\text{N}_4$ by using different precursors. Di-cyandiamide and urea at about 320 °C can be formed melamine by thermal polymerization [47]. In addition, some melamine molecules are sublimated at about 335 °C and can be polymerized at 389 °C to form a polymeric melem [64]. However, sodium nitrate can decompose at temperatures above 380 °C to produce sodium nitrite and oxygen, and has strong burning explosion and oxidizing properties, which may destroy the aromatic unit during the formation of the polymeric melem to form a $\text{C}\equiv\text{N}$ bond, which can be confirmed from FTIR [35]. Therefore, with the temperature rise, the partial destruction of the aromatic unit of the polymeric melem and complete polymeric melem further polymerization to form triazine-ring structured $\text{g-C}_3\text{N}_4$. Meanwhile, as can be seen from SEM and BET, with the participation of sodium nitrate in the thermal polymerization will increase the release of gas, which will produce a special surface. In the process of thermal polymerization, some Na^+ may be due to the role of charge will be embedded in the $\text{g-C}_3\text{N}_4$ layers of voids or spaces [22,49,64]. It is interesting to note that sodium nitrate plays a very important role in some aspects:(1) can

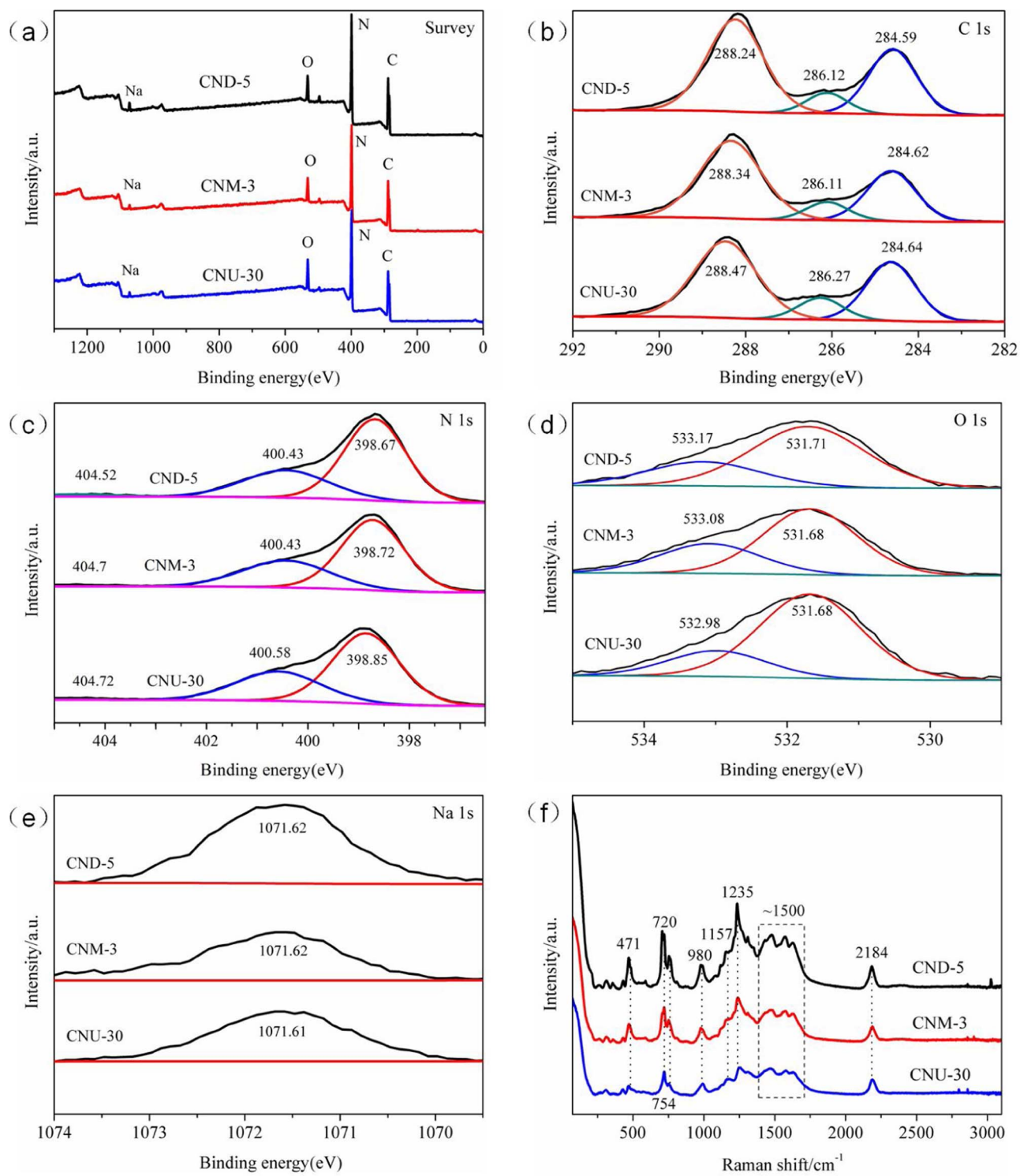


Fig. 6. (a) XPS survey spectra, (b) C 1s, (c) O 1s, (d) N 1s and Raman spectroscopy high-resolutions of CND-5, CNM-3 and CNU-30.

release a lot of gas to form a special surface; (2) can prevent aggregation in the initial coalescence to inhibit crystal growth, form a tight crystal structure [46]; (3) some of the aromatic unit of the g-C₃N₄ may be destroyed; (4) can enhance the absorption of visible light to improve the photocatalytic activity.

During photocatalytic degradation process, the h⁺, ·OH and ·O²⁻ are usually considered to be the reactive oxidative species responsible for the photo-degradation activity [28,33]. In order to elucidate the photocatalytic mechanism of as-synthesized composites, quenching experiments were performed, in which isopropanol (ISO),

benzoquinone (BQ) and ammonium oxalate (AO) were used as ·OH, ·O²⁻ and h⁺ scavengers, respectively, the result is shown in Fig. 11(a-c). As shown in Fig. 11(a and b), for the catalyst CND-5 and CNM-3, the addition of ISO induces a small change in the photocatalytic degradation efficiencies of TYL. However, under the addition of AO and BQ, there is significantly inhibit of the degradation of TYL under the same condition, indicating that the h⁺ and ·O²⁻ play a major role in the degradation of TYL. In addition, for the radical scavenger experiments of CNU-30 can be concluded that the addition of BQ is more inhibited than that of AO. Therefore, it is known that the main active species

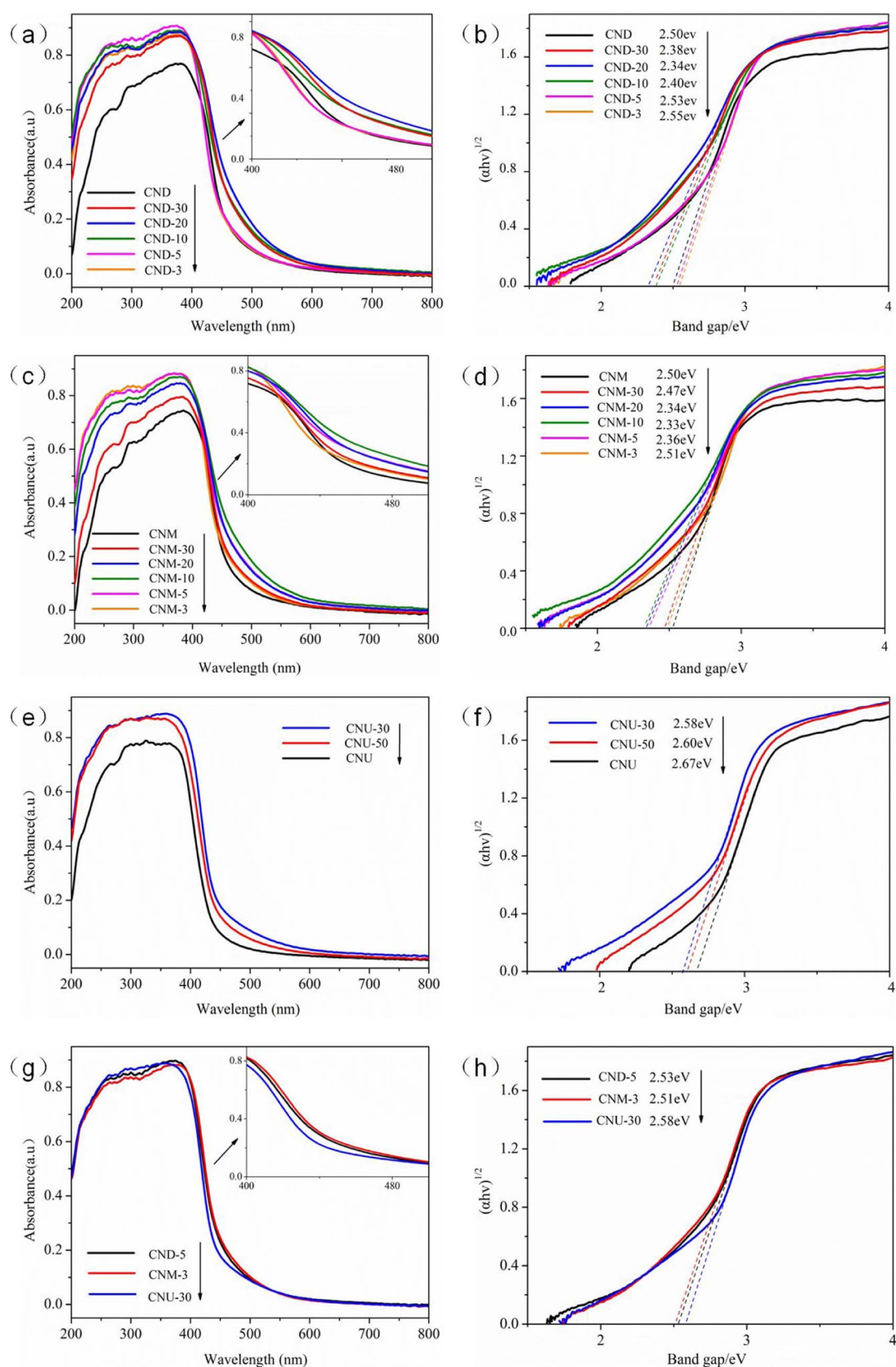


Fig. 7. UV-vis diffuse reflectance spectra, plots of $(ahv)^{1/2}$ vs photon energy of carbon nitride derived from different precursors.

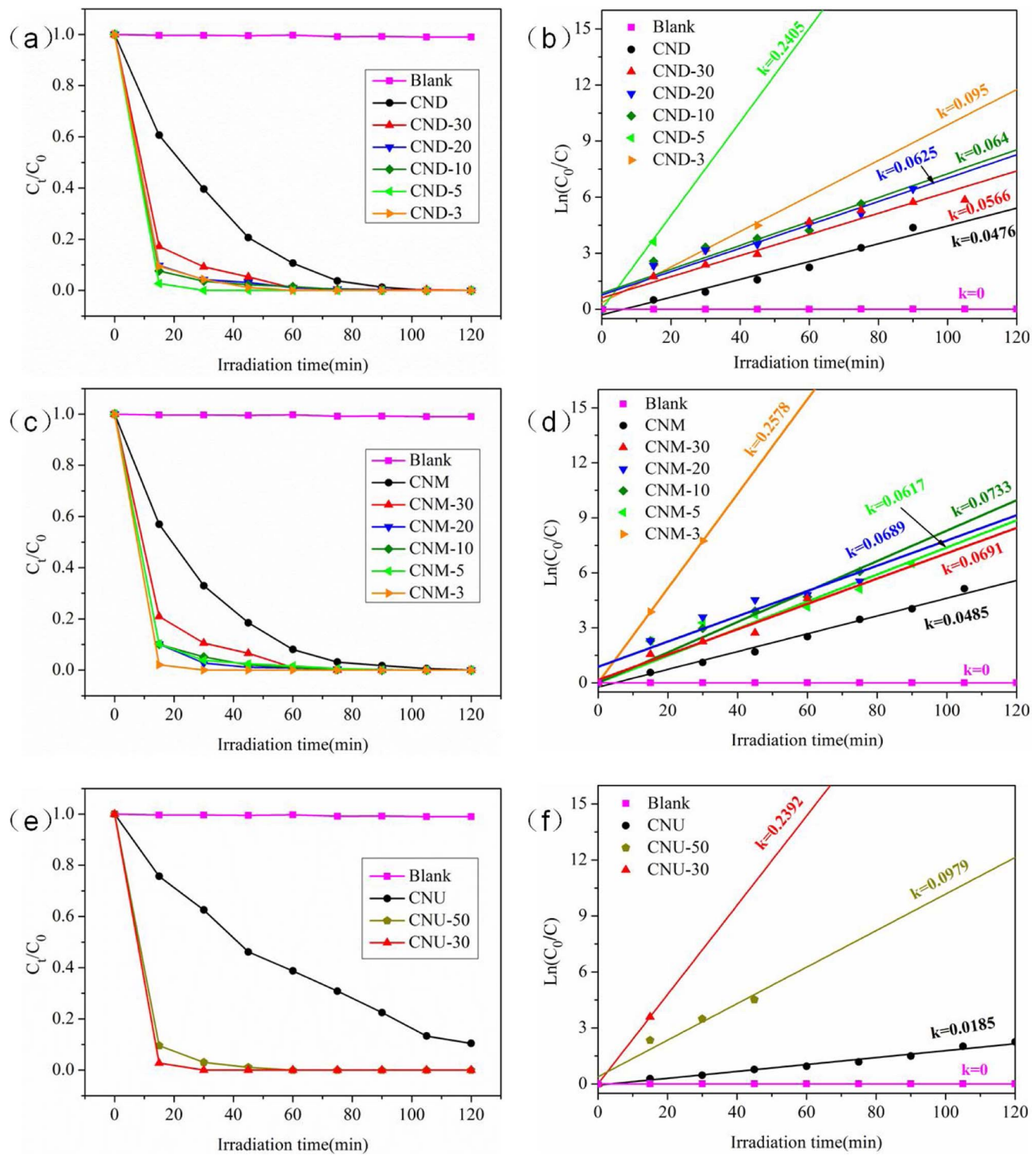


Fig. 8. time-course variation of C/C_0 and $\ln(C_0/C)$ of TYL solution under visible light illumination over CND-x(a,b), CNM-x(c,d) and CNU-x(e,f).

produced in photocatalytic reactions are $\cdot\text{O}_2^-$ and h^+ , and $\cdot\text{O}_2^-$ plays a significantly important role. Based on previous studies, the role of the reactive species $\cdot\text{OH}$ on the degradation of TYL is very small, which may be attributed to the valence band of $\text{g-C}_3\text{N}_4$ (1.57 eV vs. NHE) is less than $\cdot\text{OH}/\text{OH}^-$ (1.99 eV vs. NHE), resulting in low excitation of $\cdot\text{OH}$ [44,70,71]. In order to further explore the mechanism of photo-degradation, the effect of pH on the degradation of TYL was studied. As shown in Fig. 11(d), with the pH value increases, the photocatalytic degradation rate first increases and then decreases. The observed results were attributed to the characteristics of the TYL and the photocatalyst. At low pH values ($\text{pH} < 7.1$), with the pH value of the

solution decreases, the TYL molecule concentration decreases, and the main form of TYL species is TYL^+ [39]. Therefore, with the decrease of pH value, $\cdot\text{O}_2^-$ will combine with H^+ to produce H_2O_2 , which inhibiting the degradation of TYL:



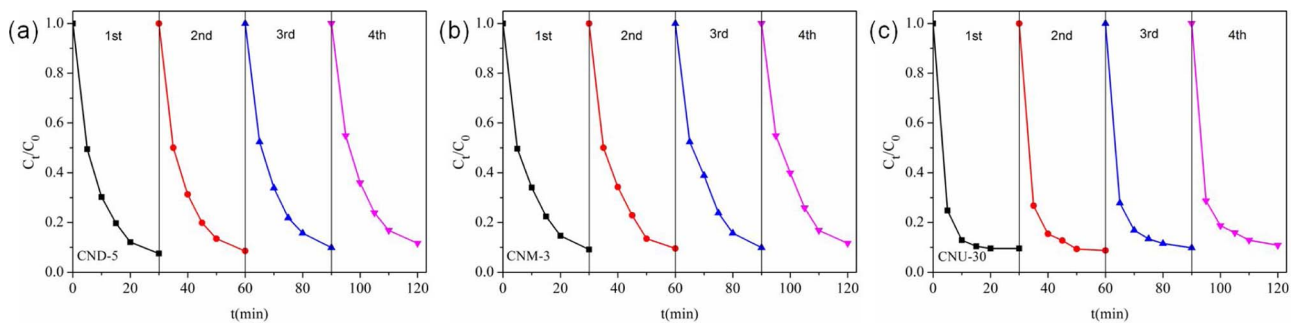
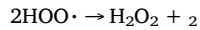
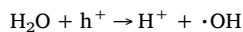


Fig. 9. Cycling runs for the photo-degradation of TYL by CND-5(a), CNM-3(b) and CNU-30(c).

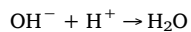


(6)

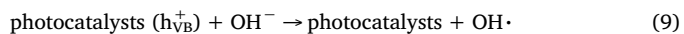
In addition, with the increase of pH value, the photodegradation activity of TYL is reduced. Thus it is reasonable to suggest that OH^- can consume part of the h^+ active group [46]:



(7)

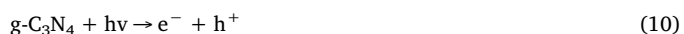


(8)

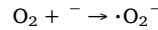


(9)

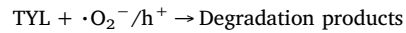
Based on the above experimental results, the photodegradation mechanism of as-prepared composites was proposed and the results are shown in Fig. 12, the process of charge transfer and degradation may be as follows:



(10)



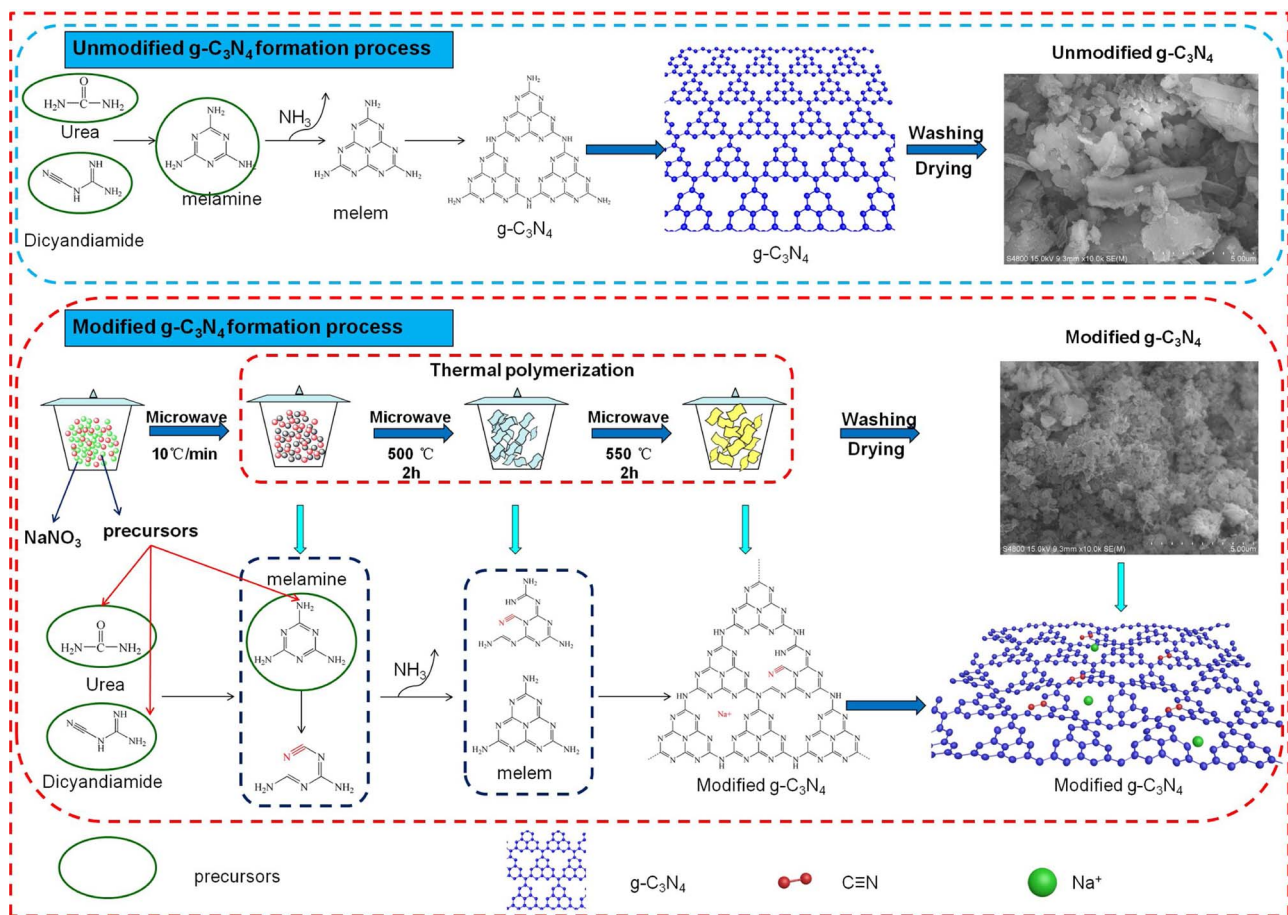
(11)



(12)

4. Conclusions

In this study, CND-x, CNM-x and CNU-x composites with well structure was synthesized by the mixture of sodium nitrate and precursor. It was found that the type of precursors and the molar ratio of sodium nitrate have an evident impact on the crystal structure of $\text{g-C}_3\text{N}_4$ and photocatalytic performance, due to different reaction pathways and degrees of condensation. Sodium nitrate alters the crystalline structure of $\text{g-C}_3\text{N}_4$ and produces new chemical bonds. It is proposed that the $\text{g-C}_3\text{N}_4$ inducing physicochemical changes are responsible for the excellent catalytic performance. In addition, as-synthesized photocatalysts exhibits high photocatalytic efficiency and excellent

Fig. 10. Possible formation mechanism of pure $\text{g-C}_3\text{N}_4$ and sodium nitrate modified $\text{g-C}_3\text{N}_4$ process.

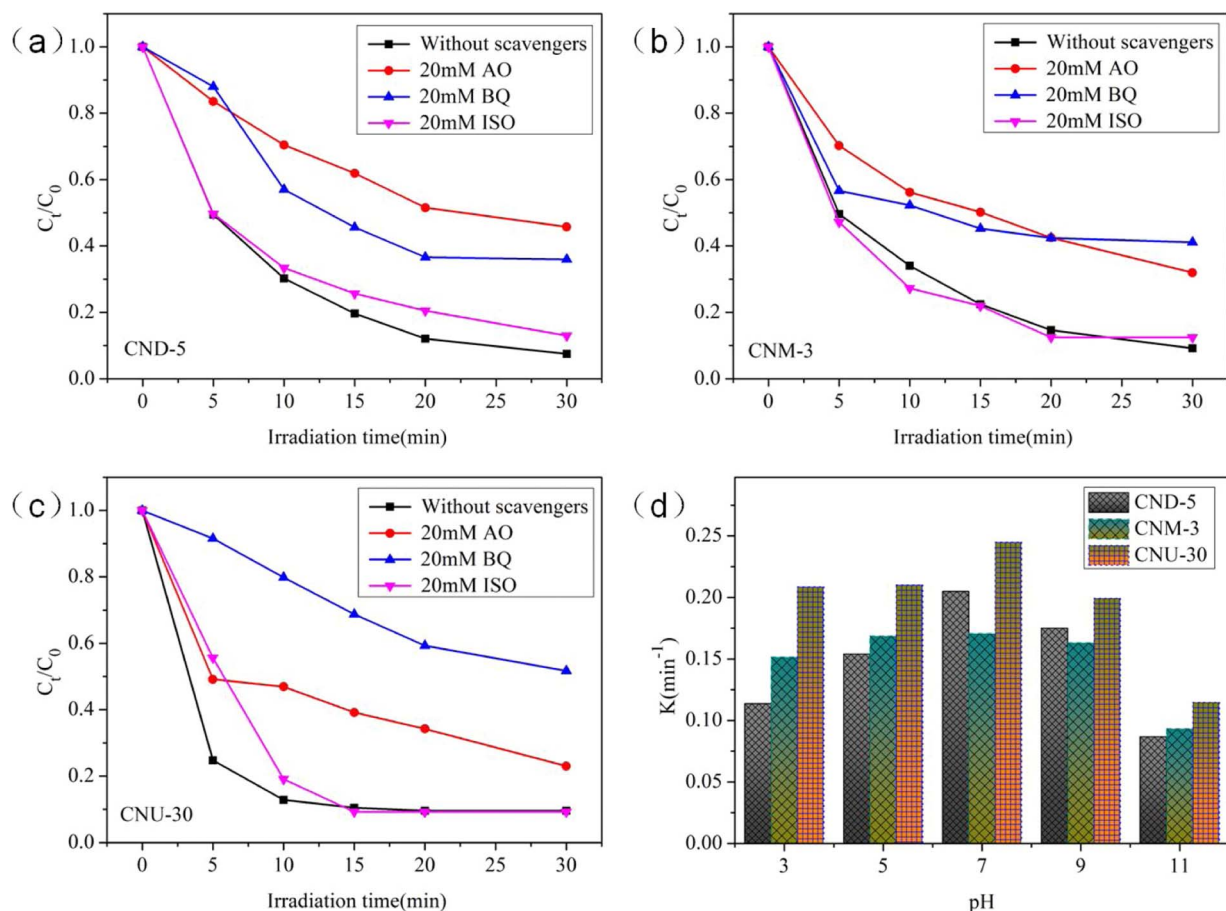


Fig. 11. Photocatalytic degradation of TYL by the CND-5(a),CNM-3(b) and CNU-30(c) under simulated solar light irradiation in the presence of different radical scavenging species;(d) Effects of pH on the rate of TYL photodegradation.

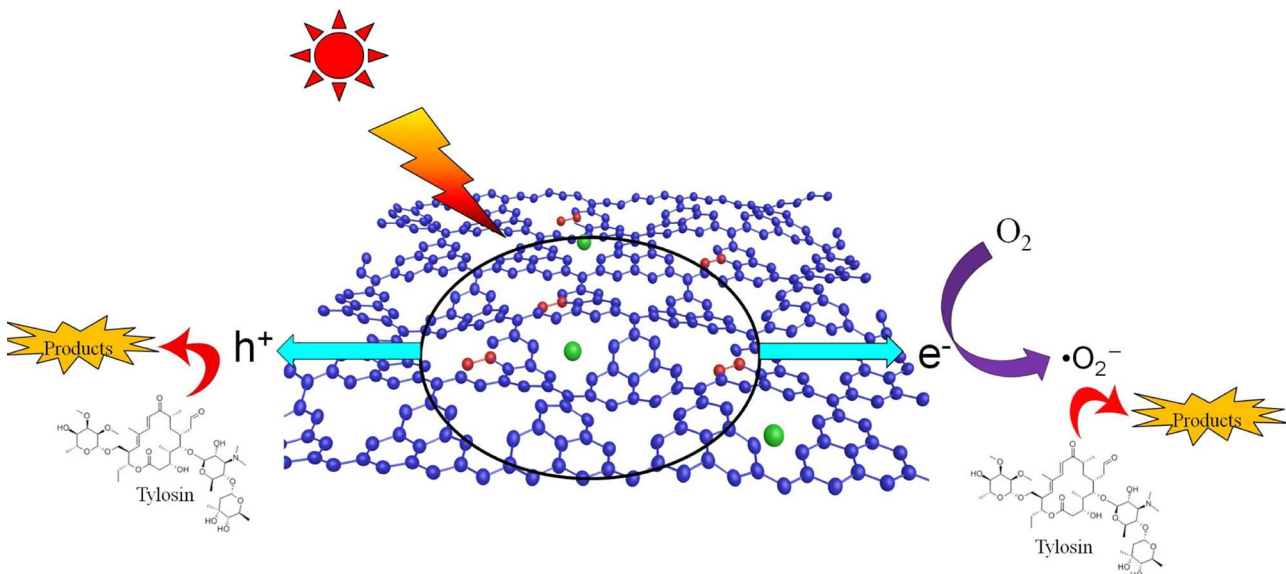


Fig. 12. Proposed mechanism of the photocatalytic degradation of TYL for the modified $\text{g-C}_3\text{N}_4$.

photocatalytic stability. Under the simulated sunlight, TYL was completely photo-degradation within 30 min, and the degradation efficiency of modified $\text{g-C}_3\text{N}_4$ was several times higher than that of pure $\text{g-C}_3\text{N}_4$. In addition, the quenching effects of different scavengers displayed that the reactive h^+ and $\cdot\text{O}_2^-$ played major role in the reaction systems. The cycling experiments determined the stability and

reusability of the samples. The composite may be used for photocatalytic degradation of antibiotics wastewater in the future.

Acknowledgements

The study was financially supported by the China National Science

Fund Program (No. 41503095), Science and Technology Planning Project of Guangdong Province, China (2016B020242004), the China Postdoctoral Science Foundation funded project (No. 2016M601994) and the Initiative Funding Programs for Doctoral Research of Northwest A&F University (Z111021702).

References

- [1] X.H. Wang, A.Y. Lin, Environ. Sci. Technol. 46 (2012) 12417–12426.
- [2] A. Pruden, M. Arabi, H.N. Storteboom, Environ. Sci. Technol. 46 (2012) 11541–11549.
- [3] Q.L. Chen, H. Li, X.Y. Zhou, Y. Zhao, J.Q. Su, X. Zhang, F.Y. Huang, Sci. Total Environ. 609 (2017) 966–973.
- [4] M. Vithanage, A.U. Rajapaksha, X. Tang, S. Thiele-Bruhn, K.H. Kim, S.-E. Lee, Y.S. Ok, J. Environ. Manage. 141 (2014) 95–103.
- [5] P. Liao, Z. Zhan, J. Dai, X. Wu, W. Zhang, K. Wang, S. Yuan, Chem. Eng. J. 228 (2013) 496–505.
- [6] A. Pruden, Environ. Sci. Technol. 48 (2014) 5–14.
- [7] M. Jia, F. Wang, Y. Bian, X. Jin, Y. Song, F.O. Kengara, R. Xu, X. Jiang, Bioresour. Technol. 136 (2013) 87–93.
- [8] J. Zhao, C. Li, R. Mezzenga, J. Phys. Condens. Matter Inst. Phys. J. 26 (2014) 464112.
- [9] S.A. Sassman, A.K. Sarmah, L.S. Lee, Environ. Toxicol. Chem. 26 (2007) 1629–1635.
- [10] W. Liu, J. Zhang, C. Zhang, L. Ren, Chem. Eng. J. 171 (2011) 431–438.
- [11] I.T. Carvalho, L. Santos, Environ. Int. 94 (2016) 736–757.
- [12] J. Wang, L. Tang, G. Zeng, Y. Deng, Y. Liu, L. Wang, Y. Zhou, Z. Guo, J. Wang, C. Zhang, Appl. Catal. B Environ. 209 (2017) 285–294.
- [13] S. Dong, X. Ding, T. Guo, X. Yue, X. Han, J. Sun, Chem. Eng. J. 316 (2017) 778–789.
- [14] J. Zhao, S. Bolisetty, S. Isabettini, J. Kohlbrecher, J. Adamcik, P. Fischer, R. Mezzenga, Biomacromolecules 17 (2016) 2555–2561.
- [15] H. Zhang, L. Zhao, F. Geng, L.-H. Guo, B. Wan, Y. Yang, Appl. Catal. B Environ. 180 (2016) 656–662.
- [16] B. Li, B. Zhang, S. Nie, L. Shao, L. Hu, J. Catal. 348 (2017) 256–264.
- [17] M. Wu, J.-M. Yan, X.-w. Zhang, M. Zhao, Appl. Surf. Sci. 354 (2015) 196–200.
- [18] A. Akhundi, A. Habibi-Yangjeh, Appl. Surf. Sci. 358 (2015) 261–269.
- [19] F. Dong, Z. Zhao, T. Xiong, Z. Ni, W. Zhang, Y. Sun, W.K. Ho, ACS Appl. Mater. Interfaces 5 (2013) 11392–11401.
- [20] I. Papailias, T. Giannakopoulou, N. Todorova, D. Demotikali, T. Vaimakis, C. Trapalis, Appl. Surf. Sci. 358 (2015) 278–286.
- [21] K. Chen, Z. Chai, C. Li, L. Shi, M. Liu, Q. Xie, Y. Zhang, D. Xu, A. Manivannan, Z. Liu, ACS Nano 10 (2016) 3665–3673.
- [22] W.-D. Oh, V.W.C. Chang, Z.-T. Hu, R. Goei, T.-T. Lim, Chem. Eng. J. 323 (2017) 260–269.
- [23] K. Li, B. Peng, J. Jin, L. Zan, T. Peng, Appl. Catal. B Environ. 203 (2017) 910–916.
- [24] J. Zhao, S. Bolisetty, J. Adamcik, J. Han, M.P. Fernandez-Ronco, R. Mezzenga, Langmuir 32 (2016) 2492–2499.
- [25] X. She, J. Wu, H. Xu, Z. Mo, J. Lian, Y. Song, L. Liu, D. Du, H. Li, Appl. Catal. B Environ. 202 (2017) 112–117.
- [26] X. Bu, J. Li, S. Yang, J. Sun, Y. Deng, Y. Yang, G. Wang, Z. Peng, P. He, X. Wang, G. Ding, J. Yang, X. Xie, ACS Appl. Mater. Interfaces 8 (2016) 31419–31425.
- [27] S. Hu, X. Chen, Q. Li, F. Li, Z. Fan, H. Wang, Y. Wang, B. Zheng, G. Wu, Appl. Catal. B Environ. 201 (2017) 58–69.
- [28] S. Ma, S. Zhan, Y. Jia, Q. Shi, Q. Zhou, Appl. Catal. B Environ. 186 (2016) 77–87.
- [29] M. Zhang, W. Jiang, D. Liu, J. Wang, Y. Liu, Y. Zhu, Y. Zhu, Appl. Catal. B Environ. 183 (2016) 263–268.
- [30] D. Jiang, T. Wang, Q. Xu, D. Li, S. Meng, M. Chen, Appl. Catal. B Environ. 201 (2017) 617–628.
- [31] X. Wu, C. Liu, X. Li, X. Zhang, C. Wang, Y. Liu, Mater. Sci. Semicond. Process. 32 (2015) 76–81.
- [32] A. Naseri, M. Samadi, A. Pourjavadi, A.Z. Moshfegh, S. Ramakrishna, J. Mater. Chem. A 5 (2017) 23406–23433.
- [33] X. Yang, F. Qian, G. Zou, M. Li, J. Lu, Y. Li, M. Bao, Appl. Catal. B Environ. 193 (2016) 22–35.
- [34] Y. Chen, B. Lin, H. Wang, Y. Yang, H. Zhu, W. Yu, J.-m. Basset, Chem. Eng. J. 286 (2016) 339–346.
- [35] T. Bauer, D. Laing, R. Tamme, Int. J. Thermophys. 33 (2011) 91–104.
- [36] S. Cao, J. Low, J. Yu, M. Jaroniec, Adv. Mater. 27 (2015) 2150–2176.
- [37] X. Guo, H. Dong, C. Yang, Q. Zhang, C. Liao, F. Zha, L. Gao, Colloids Surf. A Physicochem. Eng. Asp. 502 (2016) 81–88.
- [38] X. Guo, C. Yang, Z. Dang, Q. Zhang, Y. Li, Q. Meng, Chem. Eng. J. 223 (2013) 59–67.
- [39] X. Guo, C. Yang, Y. Wu, Z. Dang, Environ. Sci. Pollut. Res. 21 (2014) 2572–2580.
- [40] J.Y. Hu, K. Tian, H. Jiang, Chemosphere 148 (2016) 34–40.
- [41] S. Kang, L. Zhang, C. Yin, Y. Li, L. Cui, Y. Wang, Appl. Catal. B Environ. 211 (2017) 266–274.
- [42] Z.-A. Lan, G. Zhang, X. Wang, Appl. Catal. B Environ. 192 (2016) 116–125.
- [43] C. Lu, P. Zhang, S. Jiang, X. Wu, S. Song, M. Zhu, Z. Lou, Z. Li, F. Liu, Y. Liu, Y. Wang, Z. Le, Appl. Catal. B Environ. 200 (2017) 378–385.
- [44] Q. Liu, Y. Guo, Z. Chen, Z. Zhang, X. Fang, Appl. Catal. B Environ. 183 (2016) 231–241.
- [45] J. Qin, H. Zeng, Appl. Catal. B Environ. 209 (2017) 161–173.
- [46] G. Mamba, A.K. Mishra, Appl. Catal. B Environ. 198 (2016) 347–377.
- [47] Y. Zheng, Z. Zhang, C. Li, J. Photochem. Photobiol. A Chem. 332 (2017) 32–44.
- [48] J.-P. Zou, L.-C. Wang, J. Luo, Y.-C. Nie, Q.-J. Xing, X.-B. Luo, H.-M. Du, S.-L. Luo, S.L. Suib, Appl. Catal. B Environ. 193 (2016) 103–109.
- [49] W. Fang, J. Liu, L. Yu, Z. Jiang, W. Shangguan, Appl. Catal. B Environ. 209 (2017) 631–636.
- [50] Q. Xu, B. Cheng, J. Yu, G. Liu, Carbon 118 (2017) 241–249.
- [51] R.A. Rather, S. Singh, B. Pal, Appl. Catal. B Environ. 213 (2017) 9–17.
- [52] L. Yang, J. Huang, L. Shi, L. Cao, Q. Yu, Y. Jie, J. Fei, H. Ouyang, J. Ye, Appl. Catal. B Environ. 204 (2017) 335–345.
- [53] B. Li, Y. Hao, B. Zhang, X. Shao, L. Hu, Appl. Catal. A 531 (2017) 1–12.
- [54] M. Faisal, A.A. Ismail, F.A. Harraz, S.A. Al-Sayari, A.M. El-Toni, M.S. Al-Assiri, Mater. Des. 98 (2016) 223–230.
- [55] J. Yan, C. Zhou, P. Li, B. Chen, S. Zhang, X. Dong, F. Xi, J. Liu, Colloids Surf. A Physicochem. Eng. Asp. 508 (2016) 257–264.
- [56] M. Wei, L. Gao, J. Li, J. Fang, W. Cai, X. Li, A. Xu, J. Hazard. Mater. 316 (2016) 60–68.
- [57] B. Yue, Q. Li, H. Iwai, T. Kako, J. Ye, Sci. Technol. Adv. Mater. 12 (2011) 034401.
- [58] Q. Guo, Y. Xie, X. Wang, S. Zhang, T. Hou, S. Lv, Chem. Commun. (2004) 26–27.
- [59] Y. Cui, Y. Tang, X. Wang, Mater. Lett. 161 (2015) 197–200.
- [60] J. Lei, Y. Chen, F. Shen, L. Wang, Y. Liu, J. Zhang, J. Alloys Compd. 631 (2015) 328–334.
- [61] D. Xiao, K. Dai, Y. Qu, Y. Yin, H. Chen, Appl. Surf. Sci. 358 (2015) 181–187.
- [62] Z. Meng, Y. Xie, T. Cai, Z. Sun, K. Jiang, W.-Q. Han, Electrochim. Acta 210 (2016) 829–836.
- [63] L. Ma, H. Fan, J. Wang, Y. Zhao, H. Tian, G. Dong, Appl. Catal. B Environ. 190 (2016) 93–102.
- [64] H. Liu, D. Chen, Z. Wang, H. Jing, R. Zhang, Appl. Catal. B Environ. 203 (2017) 300–313.
- [65] F. Guo, J. Chen, M. Zhang, B. Gao, B. Lin, Y. Chen, J. Mater. Chem. A 4 (2016) 10806–10809.
- [66] Z. Zhu, Z. Lu, D. Wang, X. Tang, Y. Yan, W. Shi, Y. Wang, N. Gao, X. Yao, H. Dong, Appl. Catal. B Environ. 182 (2016) 115–122.
- [67] S. Liu, J. Ke, H. Sun, J. Liu, M.O. Tade, S. Wang, Appl. Catal. B Environ. 204 (2017) 358–364.
- [68] H. Zhao, S. Chen, X. Quan, H. Yu, H. Zhao, Appl. Catal. B Environ. 194 (2016) 134–140.
- [69] W. Li, C. Feng, S. Dai, J. Yue, F. Hua, H. Hou, Appl. Catal. B Environ. 168–169 (2015) 465–471.
- [70] W.-K. Jo, T.S. Natarajan, Chem. Eng. J. 281 (2015) 549–565.
- [71] X. Wang, A. Wang, J. Ma, J. Hazard. Mater. 336 (2017) 81–92.